Journal of Structural Geology, Vol. 3, No. 1, pp. 67 to 75, 1981
Printed in Great Britain

0191-8141/81/010067-08 $02.00/0

The effect of the basal–prism mechanism switch on fabric development during plastic deformation of quartzite

G. S. LISTER

Department of Structural and Applied Geology, Institute for Earth Sciences,
University of Utrecht, Uithof, Utrecht, The Netherlands

(*Received* 26 *February* 1980; *accepted in revised form* 11 *November* 1980)

Abstract—Blacic described a transition from basal ⟨*a*⟩ to prism ⟨*c*⟩ dislocation glide systems as temperature increased or strain-rate decreased in sequences of experiments involving deformation of single crystals of quartz. In this paper theoretical aspects of competition between these systems during plastic deformation are discussed. It is concluded that the basal–prism mechanism switch should have important consequences for the development of crystallographic fabrics during plastic deformation of quartzite, and the Taylor–Bishop–Hill analysis is used in an attempt to predict expected fabric transitions.

INTRODUCTION

EXPERIMENTAL work concerned with the deformation of single crystals of quartz usually reports on circumstances in which the basal ⟨*a*⟩ and prism ⟨*c*⟩ dislocation glide systems appear to play an important role (e.g. Morrison–Smith *et al.* 1976). Blacic (1975) discussed the competition between basal ⟨*a*⟩ and prism ⟨*c*⟩ glide systems during experimental deformation of quartz single crystals, and confirmed earlier reports that prism glide took over from basal glide at higher temperatures or lower strain-rates (Hobbs 1968, Baëta & Ashbee 1969, 1970, Avé L'Allement & Carter 1971, Tullis *et al.* 1973).

It is interesting to attempt to determine whether or not the basal–prism mechanism switch takes place under conditions applicable to the crustal deformation of quartzite. There are at least three ways to proceed:

(a) electron microscopic examination of naturally deformed quartzites, hoping that some record allowing definition of the deformation mechanism resides in that portion of the microstructure which survives crystal–plastic deformation and is preserved while the rock is excavated;

(b) experimental deformation of quartzite under different conditions to determine the variations of mean stress, deviatoric stress, temperature and impurity content that lead to the mechanism switch, and attempting to apply these results to natural deformations;

(c) attempting to demonstrate that certain crystallographic fabrics in naturally deformed quartzite are characteristic of the operation of prism ⟨*c*⟩ systems.

Each approach has serious drawbacks. Interpretation of electron micrographs is hindered by complex temperature, strain-rate and stress histories implicit in even the most simple tectonic event. Because crystal grains are elastically anisotropic even the relief of confining pressure generates deviatoric strains and in consequences deviatoric stresses are set up which can initiate plastic strains. Experimental data are difficult to extrapolate to natural deformations because the exact role of trace impurity content in affecting dislocation mobility is not understood, and because natural deformations involve such slow rates of strain. The interpretation of fabric data is never straightforward but crystallographic fabrics are less susceptible to vagaries of the last stages of the deformation history than is the defect substructure. For this reason the last approach may have some merit.

In this paper I set out some predictions as to how fabrics will develop in plastically deforming quartzites when prism ⟨*c*⟩ systems operate. The simple model of a crystal with one slip system deformed between flat frictionless pistons can be used to predict that the operation of basal ⟨*a*⟩ systems leads to the migration of *c*-axes away from the axis of extension, with consequent development of pole-free areas on a *c*-axis plot. Prism ⟨*c*⟩ slip would lead to the opposite result and *c*-axes would cluster near the orientation of the extension axis. Diffuse *c*-axis fabrics would be predicted for the simultaneous operation of basal and prism systems.

Predictions based on the theory of the plastic yield surface are a little more difficult to discuss. First the competition between basal ⟨*a*⟩ and prism ⟨*c*⟩ glide systems will be examined in terms of such theory, then the Taylor–Bishop–Hill analysis will be used to perform simulations of fabric development to illustrate the transitions which can occur. In assessing this work it should not be forgotten that the Taylor–Bishop–Hill analysis makes several assumptions that are untenable. Note also that critical resolved shear stress (CRSS) values are not appropriate to deformation under low stress intensities, and the effect of strictly homogeneous strain is to eliminate important reorienting mechanisms such as result when a single slip system dominates deformation (e.g. as in the model of Etchecopar 1977).

THE SINGLE CRYSTAL YIELD SURFACE AND FABRIC TRANSITIONS

Once a CRSS is specified for each possible dislocation glide system in a material several linear inequalities can be

formulated, each one demanding that the stress state in the material always lies to one side of a particular yield constraint hyperplane (Lister & Paterson 1979). In this way a region of allowable stress states bounded by a polygonal yield surface is defined. Only for stress states on the yield surface can the material deform so the vertices of the yield surface define which mechanisms can act simultaneously. The single crystal yield surface consists of polygonal segments of those constraint hyperplanes closest to the origin, that is the constraints corresponding to glide systems with lowest CRSS values.

Geometry of the basal–prism competition

The basal $\langle a \rangle$ systems are orthogonally related to the prism $\langle c \rangle$ systems. Hence these mechanisms compete at all times directly against each other with the outcome of the competition being determined solely by relative strength. The issue is not clouded by geometrical considerations as would be the case if one set of systems produced infinitesimal strains which the other could not, or if particular orientations of the stress axes relative to crystal axes disposed, say, the basal plane so that significantly higher resolved shear stresses acted in $\langle a \rangle$ directions compared with the shear stresses resolved on prism planes in $\langle c \rangle$ directions. The shear stresses resolved on the $\{0001\}\langle a \rangle$ glide systems for example are at all times identical with the shear stresses resolved on the $\{2\bar{1}\bar{1}0\}\langle c \rangle$ glide systems and both systems produce identical infinitesimal strain tensors (see Lister *et al.* 1978, appendix).

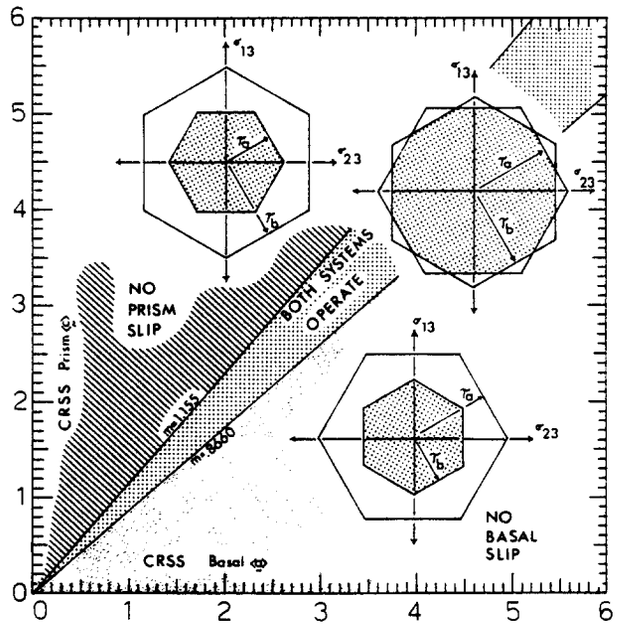

Fig. 1. Competition between the $\{0001\}\langle a \rangle$ and the $\{10\bar{1}0\}\langle c \rangle$ dislocation glide systems according to the theory of the plastic surface. Yield constraint surfaces for the two symmetry sets of glide systems are inset, showing the effect of different relative CRSS values on the topology of the yield surface in a σ_{13}, σ_{23} section of stress space. Depending on the ratio τ_a/τ_b of the CRSS values for the basal and prism systems, respectively, the two sets of yield constraint hyperplanes intersect to form either of three possible yield surface configurations. Transitions between these configurations occur at critical ratios of CRSS values.

It is therefore possible to use a much simpler method to discover fabric transitions than was used by Lister & Paterson (1979). The geometry of the basal $\langle a \rangle$/prism $\langle c \rangle$ competition can be examined directly using a technique described by Chin & Mammel (1970). The yield constraints for these glide mechanisms are determined using the Bond transformation (Terpstra & Codd 1961) and are found to be orthogonal to the σ_{12}, σ_{23} plane of 6-dimensional stress space (Fig. 1). The geometrical form of the yield constraints can therefore be displayed graphically in this section of stress space, and the effect of varying the relative CRSS values can be determined by examining the geometrical relations between the form surfaces for each mechanism subset. In the case illustrated this leads to a particularly simple pattern of fabric transitions.

Figure 1 shows that in terms of competition between the $\{0001\}\langle a \rangle$ and $\{10\bar{1}0\}\langle c \rangle$ systems by themselves there are three yield surface configurations defined by the topology of the vertices of the three possible intersections between the constraints for the different systems. From the geometry of the relationship between the two form surfaces the yield surface configuration can be seen to change at certain critical ratios of CRSS values as defined below:

$$(\sqrt{3})/2 \leq \tau_a/\tau_b \leq 2/\sqrt{3},$$

this inequality expressing the limits to which relative CRSS values can be varied with simultaneous operation of the basal $\langle a \rangle$ and prism $\{10\bar{1}0\}\langle c \rangle$ systems still allowed (Fig. 1, central portion). The constraint planes for both prism and basal systems define two hexagons, one rotated 30° with respect to the other. If the CRSS value for the basal $\langle a \rangle$ systems, τ_a, is much smaller than the CRSS value for the prism $\{10\bar{1}0\}\langle c \rangle$ systems, τ_b, then the constraint planes for the prism systems (outermost hexagon, upper left on Fig. 1) are totally excluded from the yield surface. Only the basal systems can operate when this is the case because the yield surface includes no constraint planes for prism systems. If the CRSS value for the prism systems is much less than the CRSS value for the basal systems then the reverse situation applies (lower right of Fig. 1).

Simulations using the Taylor–Bishop–Hill analysis

Simulations of fabric development using the Taylor–Bishop–Hill analysis (Lister *et al.* 1978) have been carried out to illustrate the effects of different outcomes in the competition between basal $\langle a \rangle$ and prism $\langle c \rangle$ systems. Three sequences of simulations have been performed: (a) basal $\langle a \rangle$ glide operating without prism $\langle c \rangle$ glide (top row in each of Figs. 2–4); (b) simultaneous operation of basal $\langle a \rangle$ and prism $\langle c \rangle$ systems (middle row in each of the above figures); and (c) prism $\langle c \rangle$ systems operating without basal $\langle a \rangle$ systems (bottom row of each of the above figures).

The glide systems and the CRSS values used for fabric simulations are shown in Tables 1–2. One set of CRSS

Table 1. Dislocation glide systems used in the simulations

BASAL <A> SYSTEMS			
0 0 1	1 0 0	(0 0 0 1)	A1
0 0 1	-1 0 0	(0 0 0 1)	-A1
0 0 1	0 1 0	(0 0 0 1)	A2
0 0 1	0-1 0	(0 0 0 1)	-A2
0 0 1	-1-1 0	(0 0 0 1)	A3
0 0 1	1 1 0	(0 0 0 1)	-A3
PRISM <C> SYSTEMS			
-1 0 0	0 0 1	(-1 0 1 0)	C
-1 0 0	0 0 1	(-1 0 1 0)	C
0 1 0	0 0 1	(0 1-1 0)	C
0 1 0	0 0 1	(0 1-1 0)	C
1-1 0	0 0 1	(1-1 0 0)	C
1-1 0	0 0 1	(1-1 0 0)	C
PRISM <A> SYSTEMS			
-1 0 0	0 1 0	(-1 0 1 0)	A2
-1 0 0	0-1 0	(-1 0 1 0)	-A2
0 1 0	1 0 0	(0 1-1 0)	A1
0 1 0	-1 0 0	(0 1-1 0)	-A1
1-1 0	-1-1 0	(1-1 0 0)	A3
1-1 0	1 1 0	(1-1 0 0)	-A3
(+) RHOMB <A> SYSTEMS			
1 0 1	0 1 0	(1 0-1 1)	A2
1 0 1	0-1 0	(1 0-1 1)	-A2
0-1 1	1 0 0	(0-1 1 1)	A1
0-1 1	-1 0 0	(0-1 1 1)	-A1
-1 1 1	-1-1 0	(-1 1 0 1)	A3
-1 1 1	1 1 0	(-1 1 0 1)	-A3
(-) RHOMB <A> SYSTEMS			
-1 0 1	0 1 0	(-1 0 1 1)	A2
-1 0 1	0-1 0	(-1 0 1 1)	-A2
0 1 1	1 0 0	(0 1 1 1)	A1
0 1 1	-1 0 0	(0 1 1 1)	-A1
1-1 1	-1-1 0	(1-1 0 1)	A3
1-1 1	1 1 0	(1-1 0 1)	-A3

(+) RHOMB <C+A> SYSTEMS		
1 0 1	-1 0 1	(1 0-1 1) C-A1
1 0 1	-1-1 1	(1 0-1 1) C+A3
0-1 1	0 1 1	(0-1 1 1) C+A2
0-1 1	1 1 1	(0-1 1 1) C-A3
-1 1 1	0-1 1	(-1 1 0 1) C-A2
-1 1 1	1 0 1	(-1 1 0 1) C+A1
1 0 1	1 0-1	(1 0-1 1) -C+A1
1 0 1	1 1-1	(1 0-1 1) -C-A3
0-1 1	0-1-1	(0-1 1 1) -C-A2
0-1 1	-1-1-1	(0-1 1 1) -C+A3
-1 1 1	0 1-1	(-1 1 0 1) -C+A2
-1 1 1	-1 0-1	(-1 1 0 1) -C-A1
(-) RHOMB <C+A> SYSTEMS		
-1 0 1	1 0 1	(-1 0 1 1) C+A1
-1 0 1	1 1 1	(-1 0 1 1) C-A3
0 1 1	0-1 1	(0 1-1 1) C-A2
0 1 1	-1-1 1	(0 1-1 1) C+A3
1-1 1	0 1 1	(1-1 0 1) C+A2
1-1 1	-1 0 1	(1-1 0 1) C-A1
-1 0 1	-1 0-1	(-1 0 1 1) -C-A1
-1 0 1	-1-1-1	(-1 0 1 1) -C+A3
0 1 1	0 1-1	(0 1-1 1) -C+A2
0 1 1	1 1-1	(0 1-1 1) -C-A3
1-1 1	0-1-1	(1-1 0 1) -C-A2
1-1 1	1 0-1	(1-1 0 1) -C+A1

Table 2. CRSS values for the different model quartzites

CRITICAL RESOLVED SHEAR STRESS VALUES

			FIGURE 2			FIGURE 3			FIGURE 4		
			A 0 W 1	A 0 W 2	A 0 W 3	A 0 W 1	A 0 W 2	A 0 W 3	A 0 W 1	A 0 W 2	A 0 W 3
BASAL	<A>	---	1.0	1.0	...	1.0	1.0	...	1.0	1.0	...
PRISM	<C>	---	...	1.0	1.0	...	1.0	1.0	...	1.0	1.0
PRISM	<A>	---	1.0	1.0	1.0	...	...	...	0.1	0.1	0.1
(+) RHOMB	<A>	---	...	...	...	3.0	3.0	3.0	...	...	...
(-) RHOMB	<A>	---	1.0	1.0	1.0	3.0	3.0	3.0	1.0	1.0	1.0
(+) RHOMB	<C+A>	--	...	...	...	3.0	3.0	3.0	...	...	...
(-) RHOMB	<C+A>	--	3.0	3.0	3.0	3.0	3.0	3.0	3.0	3.0	3.0

CRITICAL RESOLVED SHEAR STRESS VALUES

			FIGURE 5				FIGURE 6	
			A 0 W 1	A 0 W 2	A 0 W 3	A 0 W 4	STAGE ONE	STAGE TWO
BASAL	<A>	---	1.0	1.0	1.0	1.0	1.0	...
PRISM	<C>	---	1.0	1.0	1.0	1.0	...	1.0
PRISM	<A>	---	1.0	0.3	0.2	0.1	0.5	0.5
(+) RHOMB	<A>	---	...	...	...	...	...	2.5
(-) RHOMB	<A>	---	1.0	1.0	1.0	1.0	2.0	2.5
(+) RHOMB	<C+A>	--	...	...	...	...	...	2.5
(-) RHOMB	<C+A>	--	3.0	3.0	3.0	3.0	2.0	2.5

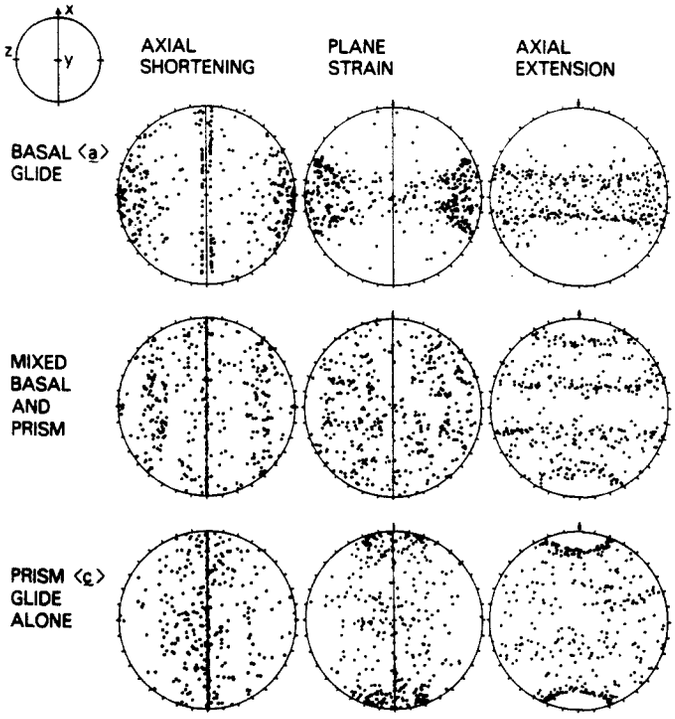

Fig. 2. The effect of the basal ⟨*a*⟩/prism ⟨*c*⟩ mechanism switch illustrated for quartz with trigonal symmetry. All ⟨*a*⟩ glide systems have equal CRSS values. Note the almost random fabric for plane strain when the basal and prism mechanisms both operate. CRSS values in Table 2.

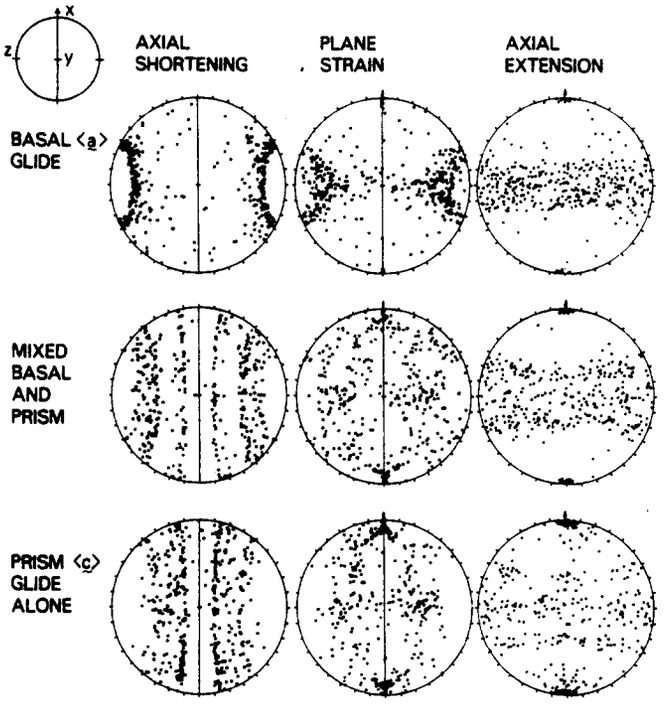

Fig. 3. The effect of the basal ⟨*a*⟩/prism ⟨*c*⟩ mechanism switch illustrated for quartz with hexagonal symmetry. The prism ⟨*a*⟩ systems do not operate in this simulation sequence. CRSS values in Table 2.

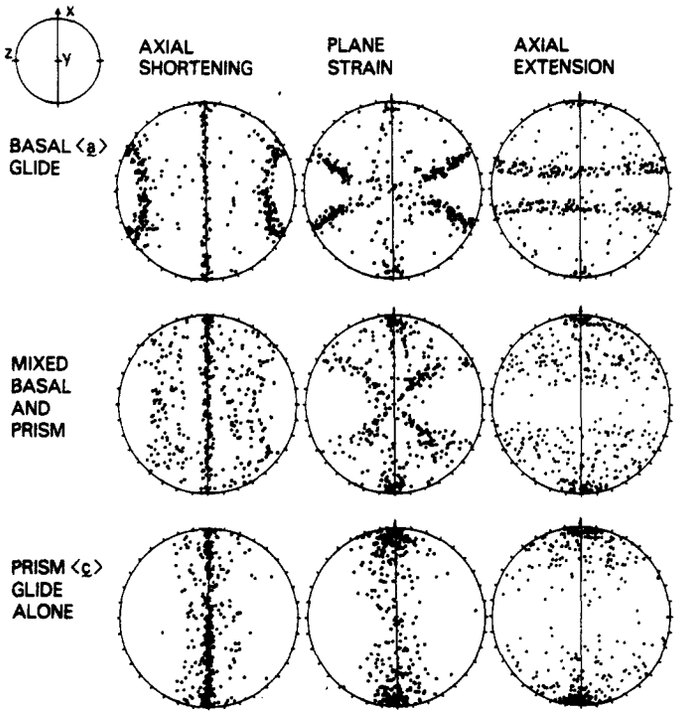

Fig. 4. The effect of the basal ⟨*a*⟩/prism ⟨*c*⟩ mechanism switch illustrated for quartz with trigonal symmetry, and for a CRSS value on the prism ⟨*a*⟩ systems set relatively very low in relation to the other systems. Note the 90° crossed-girdle centred on the *Y*-axis for mixed basal and prism slip. CRSS values in Table 2.

values defines one model quartzite. For each model quartzite 400 randomly oriented grains are subjected to each of three deformations: (a) axially symmetric shortening; (b) plane strain; and (c) axially symmetric extension. The *c*-axis fabrics that result after 65% shortening or 290% extension (as the case may be) are shown in Figs. 2–4. The following should be noted.

(a) Figure 2 shows the effect of the basal ⟨*a*⟩/prism ⟨*c*⟩ mechanism switch when all of the glide systems with ⟨*a*⟩ Burgers vector have the same CRSS values (see Table 2). The basal {0001}, prism $\{10\bar{1}0\}$, and (−) rhomb $\{01\bar{1}1\}$ ⟨*a*⟩ systems operate with CRSS value one-third that applicable on the (−) rhomb $\{01\bar{1}1\}$ ⟨*c* + *a*⟩ systems. The (+) rhomb systems do not operate at all and so the symmetry of the quartz is trigonal (as appropriate to the *alpha* field) during this sequence of simulations. The fabrics produced during axial shortening change from point-maxima of *c*-axes parallel to *Z* to 40–50° small-circle girdles around *Z* when prism ⟨*c*⟩ slip systems are introduced in addition to basal ⟨*a*⟩ systems. In plane strain simulations a double wedge fabric develops if basal ⟨*a*⟩ systems operate without prism ⟨*c*⟩ systems, but this changes to a pattern which is almost random if deformation is accomplished with simultaneous operation of basal ⟨*a*⟩ and prism ⟨*c*⟩ systems.

(b) Figure 3 shows the effect of the basal ⟨*a*⟩/prism ⟨*c*⟩ mechanism switch when glide systems operate that define a model quartz with hexagonal symmetry (as appropriate to the *beta* field). Both (+) and (−) rhomb ⟨*a*⟩ and ⟨*c* + *a*⟩ systems operate, with equal CRSS values. No prism ⟨*a*⟩ glide was allowed however. The CRSS values for the basal ⟨*a*⟩ and prism ⟨*c*⟩ systems were set at one-third of the CRSS value for the rhomb systems. Note that in comparison with Fig. 2, for axial shortening, the change from trigonal symmetry to hexagonal symmetry causes the *c*-axis fabric to develop as a 25° small-circle girdle for basal ⟨*a*⟩ systems operating without prism ⟨*c*⟩ systems.

(c) Figure 4 shows the effect of the basal ⟨*a*⟩/prism ⟨*c*⟩ mechanism switch when glide systems operate as for Fig. 2, but with the CRSS value on the prism ⟨*a*⟩ systems very small in comparison with all other CRSS values. This has many interesting effects. There is a marked increase in the percentage of *c*-axes that concentrate parallel to the axis of extension or perpendicular to the axis of shortening. When basal ⟨*a*⟩ and prism ⟨*c*⟩ systems operate simultaneously, for plane strain, a 90° crossed-girdle forms, centred on the *Y*-axis.

In nearly all simulations carried out to date there has been little variation in the *c*-axis fabrics formed when basal ⟨*a*⟩ systems have not operated, as long as prism ⟨*a*⟩ and prism ⟨*c*⟩ systems are both important glide systems in allowing the deformation process. Girdles form in the *XY* plane of the strain ellipsoid (for coaxial histories) and maxima form at the *X*-axis. It is otherwise difficult to generalize the effect that the addition of prism ⟨*c*⟩ glide systems has on the deformation fabrics produced during the model simulations.

Mixed basal ⟨*a*⟩ and prism ⟨*c*⟩ slip tends to produce 40–50° small-circle distributions of *c*-axes during axial shortening. Many *c*-axes align at right-angles to the *Z*-axis. During plane strain there is a greater variety of fabrics produced, but one important trend is discerned in

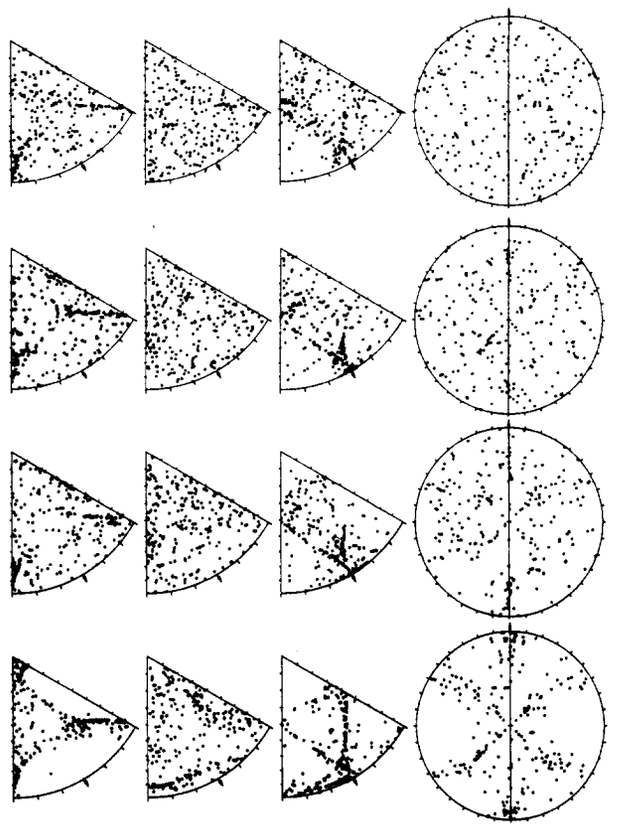

Fig. 5. Four model quartzites subjected to 60% shortening in plane strain. Each row shows from left to right the inverse pole figures (equal-area upper hemisphere) for the X, Y, and Z finite strain axes, and the c-axis pole figure for 250 grains (equal-area, lower hemisphere). Each simulation involves simultaneous operation of basal $\langle a \rangle$ and prism $\langle c \rangle$ glide systems, but from top to bottom, the CRSS on the prism $\langle a \rangle$ systems is progressively smaller. CRSS values set out in Table 2.

Fig. 5. This figure shows four different fabrics produced by plane-strain simulations. The c-axis fabrics vary from near-random (Fig. 2), when the prism $\langle a \rangle$ systems have the same CRSS value as all the other glide systems with $\langle a \rangle$ Burgers vector, to a complex pattern with a prominent 90° crossed-girdle of c-axes centred on the Y-axis when the prism $\langle a \rangle$ glide systems are relatively very easy in comparison with all other systems (Fig. 4).

It is important to realize that there are thousands of possible yield surface configurations involving competition between basal $\langle a \rangle$ and prism $\langle c \rangle$ glide systems, and there is no easy way of predicting the variation in fabric associated with all of these changes. Lister (1979) considered various two-dimensional sections of a four-dimensional configuration space, and demonstrated homeomorphic relations between different sections. In this way, for the combination of systems examined, the total variation obtained when basal $\langle a \rangle$ and prism $\langle c \rangle$ glide systems operate together in the presence of hard (−) rhomb $\langle c + a \rangle$ systems can be reduced to four model quartzites. The (−) rhomb $\langle a \rangle$ systems can be introduced into the competition without changing this result. In fact if the (−) rhomb $\langle a \rangle$ systems are allowed to operate with a CRSS value less than that applicable to the $\langle c + a \rangle$ systems, the CRSS value on the $\langle c + a \rangle$ systems ceases to have any influence in determining the yield surface configuration. The CRSS values on the systems with $\langle a \rangle$ Burgers vector totally determine the fabric that will develop.

Without prism $\langle c \rangle$ systems operating the fabrics that form generally have opening angles of less than 40°, especially considering the intersection of the skeletal lines across the Y-axis. When prism $\langle c \rangle$, prism $\langle a \rangle$ and basal $\langle a \rangle$ systems operate simultaneously this is no longer the case as has been pointed out above. Skeletal lines that intersect at right-angles across the Y-axis are then common. These tendencies are suggested as characteristic of mixed basal and prism slip, and as diagnostic of the appearance of the $\langle c \rangle$ Burgers vector during crystal-plastic deformation of quartzite.

The effect of the mechanism switch during deformation

Considerable effects can result if the basal–prism mechanism switch takes place at an intermediate stage in a deformation history, after a strong crystallographic fabric has developed. The pattern of reorientation will abruptly change and early formed maxima and girdles will migrate *en masse* towards new end-orientations. To illustrate this effect, model quartzite II of Lister *et al.* (1978) was subjected to 50% shortening in plane strain (Fig. 6a) and then the basal $\langle a \rangle$/prism $\langle c \rangle$ mechanism switch was allowed to take place. The basal systems ceased operation and the prism $\{10\bar{1}0\}\langle c \rangle$ systems were allowed to become active. At the same time the deformation path was changed to involve axially symmetric shortening (with the axis of shortening as before).

Up until the point that the mechanism switch took place a type I crossed-girdle fabric had developed. After that the opening angle of the pattern and the positions of the maxima changed by about ½° for every 1% additional shortening. This means that the crystallographic fabric is significantly modified by even small additional strains (see Figs. 6b–d), and that modifications to fabric because of the basal-prism switch take place towards the end of deformation and may be an important aspect of fabric development during natural deformation.

DISCUSSION

There are a number of the simulated patterns that appear to have no natural counterparts and even the patterns which show some resemblance to fabrics produced during orogeny differ in important details. For example, none of the simulated patterns have developed c-axis maxima parallel to the axis of intermediate shortening, and such Y-axis maxima are important aspects of many patterns of preferred orientation observed in deformed quartzites. In addition many of the simulated patterns have c-axis maxima at or near the axis of extension. If 'kinking' is included in the simulation process maxima at or near the X-axis will weaken or disappear if basal slip is important in the deformation process.

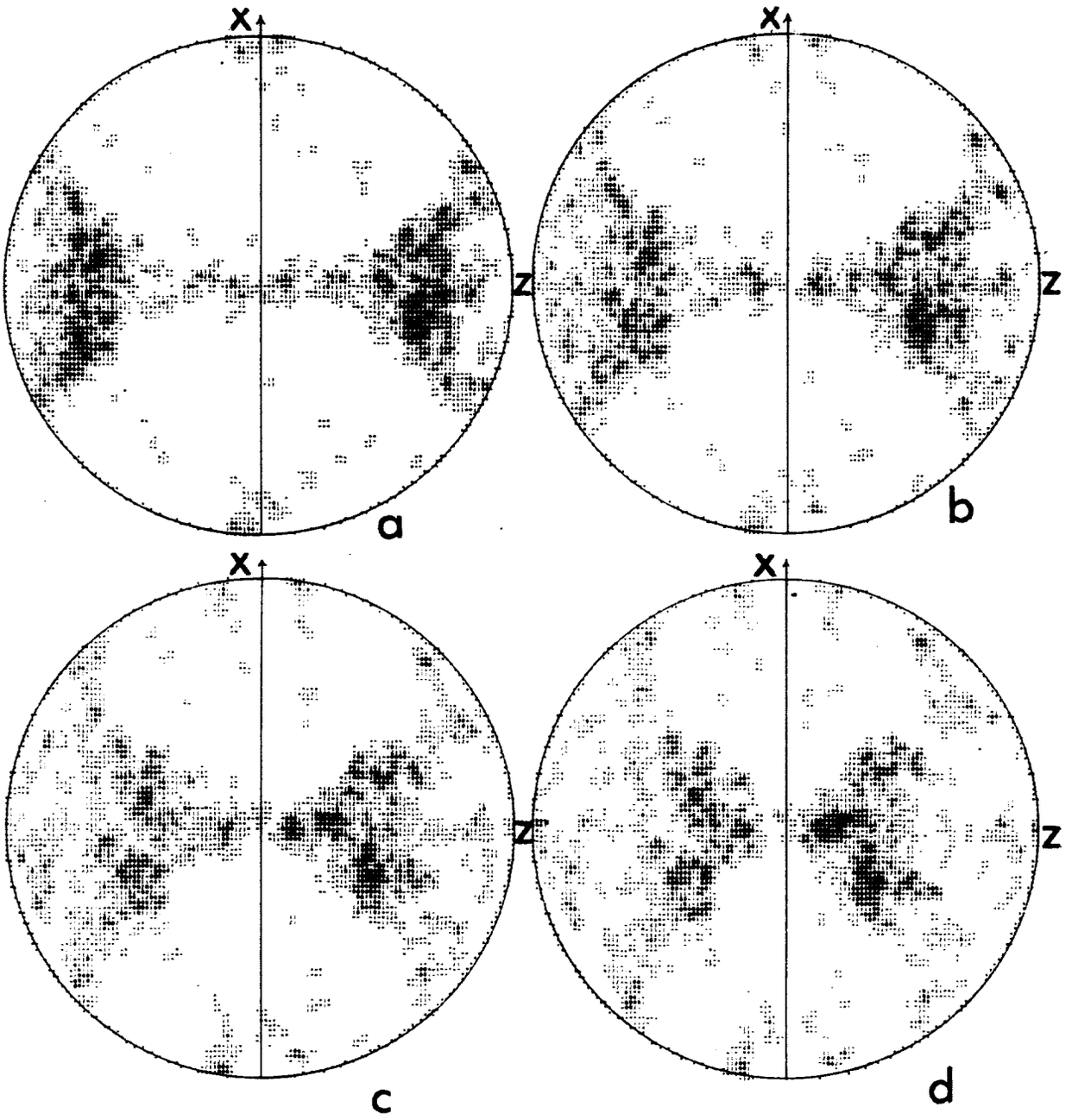

Fig. 6. A simulation of the effects of the basal–prism mechanism switch at an intermediate stage in a deformation history which has already resulted in a strong crystallographic fabric. Model quartzite II of Lister *et al.* (1978) has been subjected to 50% shortening in plane strain (a) and a type I crossed-girdle of *c*-axes has formed. CRSS values are set out in Table 2 (stage one). The basal–prism mechanism switch then takes place and basal systems cease operation. At the same time the deformation path changes to progressive axially symmetric shortening. In stage two of the deformation history the early formed fabric is rapidly modified. Opening angles increase at ths rate of $\frac{1}{2}^{\circ}$ for each additional 1% shortening. Diagrams (b), (c) and (d) show the *c*-axis fabric after 20, 40 and 60% logarithmic shortening in stage two of the deformation history.

Including such a factor will increase the degree of resemblance between the simulated fabrics and real patterns.

The most interesting part of this work can be seen by considering only the skeletal outlines of the fabric patterns. Considering only this aspect of the simulated patterns, and ignoring the actual distribution of maxima, leads to the conclusion that simulations with the Taylor–Bishop–Hill analysis produce realistic skeletal outlines, and, as noted, characteristic skeletal elements result when prism ⟨*c*⟩ and basal ⟨*a*⟩ systems are simultaneously active during deformation. It is therefore a matter of interest that similar variations in skeletal outlines are observed in the Saxony granulite terrain (Lister & Dornsiepen in preparation). Field studies may be able to use this variation to determine whether or not the basal–prism mechanism switch has occurred during natural deformation.

CONCLUSION

Fabric simulations show that important fabric variation will result from different outcomes in the competition between basal ⟨*a*⟩ and prism ⟨*c*⟩ glide systems. The basal ⟨*a*⟩ and prism ⟨*c*⟩ systems compete directly with each other during deformation and the issue is not complicated by geometrical considerations as it would be if stress axes could be oriented to stress one set of systems more highly than the others, or if one set could achieve strains which the others could not. It is suggested that a characteristic feature of the fabric skeleton produced when basal ⟨*a*⟩ and prism ⟨*c*⟩ systems operate simultaneously is a 90° crossed-girdle of *c*-axes, centred on the *Y*-axis.

If the basal–prism mechanism switch takes place during a deformation history after a strong crystallographic fabric has developed the early formed maxima and girdles rotate *en masse* toward new end-orientations. A 20% shortening after the mechanism switch has taken place can cause maxima to move more than 10° away from their original positions. Such modifications may be an important aspect of the development of crystallographic fabrics during crustal deformation of quartzite.

Acknowledgement—The author has benefited from correspondence with Jan Tullis during review.

REFERENCES

Avé L'allemant, H. G. & Carter, N. L. 1971. Pressure dependence of quartz deformation lamellae orientations. *Am. J. Sci.* **270,** 218–235.

Baëta, R. D. & Ashbee, K. H. G. 1969. Slip systems in quartz: I. experiments. *Am. Miner.* **54,** 1551–1573.

Baëta, R. D. & Ashbee, K. H. G. 1969. Slip systems in quartz: II. interpretation. *Am. Miner.* **54,** 1574–1582.

Baëta, R. D. & Ashbee, K. H. G. 1970. Mechanical deformation of quartz. I. constant strain rate compression experiments. *Phil. Mag.* **22,** 601–624.

Blacic, J. D. 1975. Plastic deformation mechanisms in quartz: the effect of water. *Tectonophysics* **27,** 271–294.

Chin, G. Y. & Mammel, W. L. 1970. Competition among basal, prism and pyramidal slip modes in HCP metals. *Metall. Trans.* **1,** 357–361.

Etchecopar, A. 1977. A plane kinematic model of progressive deformation in a polycrystalline aggregate. *Tectonophysics* **39,** 121–142.

Hobbs, B. E. 1968. Recrystallization of single crystals of quartz. *Tectonophysics* **6,** 353–401.

Lister, G. S. 1979. Fabric transitions in plastically deformed quartzites: competition between basal, prism and rhomb systems. *Bull. Mineral.* **102,** 232–241.

Lister, G. S. & Paterson, M. S. 1979. The simulation of fabric development during plastic deformation and its application to quartzite: fabric transitions. *J. Struct. Geol.* **1,** 99–115.

Lister, G. S., Paterson, M. S. & Hobbs, B. E. 1978. The simulation of fabric developments in plastic deformation and its application to quartzite: the model. *Tectonophysics* **45,** 107–158.

Terpstra, P. & Codd, L. W. 1961. *Crystallometry*. Longmans, London.

Tullis, J. A., Christie, J. M. & Griggs, D. T. 1973. Microstructures and preferred orientations of experimentally deformed quartzites. *Bull. geol. Soc. Am.* **84,** 297–314.

Morrison-Smith, D., Paterson, M. S. & Hobbs, B. E. 1976. An electron microscope study of plastic deformation in single crystals of synthetic quartz. *Tectonophysics* **33,** 43–79.